Carbon nanocages with nanographene shell for high-rate lithium ion batteries

Kaixue Wang,[†] Zhonglai Li,[§]Yonggang Wang,[¶] Haimei Liu,[¶] Jiesheng Chen,[†] Justin Holmes[§] and Haoshen Zhou[¶]

[†]*School of Chemistry and Chemical Engineering, Shanghai Jiao Tong University, Shanghai 200240, P. R. China*

[§]*Department of Chemistry and the Tyndall National Institute ,University College Cork, Cork, Ireland*

[¶]*Energy Technology Research Institute, AIST Tsukuba, Central 2, Ibaraki 305-8568, Japan*

Abstract

Carbon nanocages have been prepared by a catalytic decomposition of *p*-Xylene on a MgO supported Co and Mo catalyst in supercritical CO_2 at a pressure of 10.34 MPa and temperatures ranging from 650 to 750 ^oC. The electrochemical performance of these carbon nanocages as anodes for lithium ion batteries has been evaluated by galvanostatic cycling. The carbon nanocages prepared at a temperature of 750 ^oC exhibited relatively high reversible capacities, superior rate performance and excellent cycling life. The advanced performance of the carbon nanocages prepared at 750 ^oC is ascribed to their unique structural features: 1) the partially graphitized carbon shells and the well inter-cage contact ensuring the fast electron transportation, 2) the porous network formed by the fine pores in the carbon shell and the void space among the cages facilitating the penetration of the electrolyte and ions within the electrode, 3) the thin carbon shells shortening the diffusion distance of Li ions, and 4) the high specific surface area providing a large number of active sites for charge-transfer reactions. These carbon nanocages are promising candidate for the application in lithium ion batteries.

Introduction

Due to the capacity and safety concerns associated with pure Li metal, carbon electrode materials have received considerable attention and are playing a key role in the field of lithium ion batteries.[1-6] So far, graphite is still the most commonly used carbon electrode materials. However, the theoretical lithium storage capacity in graphite is only up to 372 mA h/g, which can not satisfy the demand for the lithium ion batteries with high energy storage capacity. Thus, there is still need to improve or optimize the carbon electrode materials to enhance the storage capacity, the cycleability and the rate performance. Usually, the chemical diffusion of lithium ions within the electrode materials is the rate-limiting step.[7,8] Therefore, much effort has been made to nanostructured carbon materials, especially to carbon materials with well-controlled dimensions and morphologies. Carbon nanotubes, including multi-walled nanotubes or nanofilaments (MWNTs)[1,9-15] and single-walled nanotubes (SWNTs)[16-18] have been studied as anode materials for lithium ion batteries. Although a high reversible capacity of 400 – 600 mA h/g can be reached, the low graphitized carbon nanotubes with high specific surface area are usually less stable during the galvanostatic cycling.[14-16,19] Moreover, for high-graphitized carbon nanotubes, long-term stability can be achieved, but the reversible capability is low, even lower than that of graphite.[15] Recently, mesoporous carbon materials prepared by a soft or hard template

method have been considered as anode materials for lithium ion batteries.[6,20-22] Taking the advantages of the high specific surface area and the well-ordered porous channel systems, mesoporous carbon materials exhibit high lithium storage capacity. However, the amorphous wall and the poor electronic conductivity of the mesoporous carbon lead to the poor cycling and rate performance.[6,20-22]

Carbon nanocages, with remarkably large mesoporous volumes, have been fabricated by the deposition of *p*-Xylene over a Co/Mo catalyst in supercritical carbon dioxide.[23] The structure of the nanocages produced can be well-controlled by tuning the reaction temperature and pressure. In this work, the electrochemical properties of these carbon nanocages for lithium ion batteries have been evaluated. These carbon nanocages with unique structure features are expected to meet the demands for the electrode materials with high storage capacity, good cycling and rate performance.

Experimental

The carbon nanocages were prepared by the deposition of *p*-Xylene over a Co/Mo catalyst in supercritical carbon dioxide as described in our previous work.[23] The surface area and pore volume of the nanocages produced were manipulated by tuning the reaction temperature and pressure employed. Typically, a quartz boat containing 0.5 g MgO supported 3 wt % Co

and 4 wt % Mo catalyst was placed in the center of a high-pressure stainless steel reactor (Inconel 625 GR2- Snap-tite, Inc.), followed by the heating treatment in a reducing atmosphere of H_2/Ar (1:9, v/v) at a flow rate of 200 mL min^{-1} for 30 min. *P*-Xylene was first added into a 450 mL stainless steel reservoir and charged with CO_2 at 40 ^oC. The gaseous mixture maintaining above the critical temperature and pressure of CO_2 flowed through reactor at a constant pressure and a controlled flow rate. The reactions were conducted at temperatures of 650, 700, and 750 ^oC, respectively, for approximately 1 h, followed by the cooling down to room temperature under an Ar flow. The carbon nanocages were obtained by treating the resulting black powder in 6 M HNO_3. The carbon nanocages prepared at temperatures of 650, 700, and 750 ^oC were denoted as CNC-650, CNC-700, and CNC-750, respectively in the context.

X-ray diffraction (XRD) patterns were recorded in a θ-2θ mode on D/max-2200/PC diffractometer from Rigaku Corp. Japan. The morphology of the carbon nanofiber arrays was characterized by scanning electron microscopy (SEM) performed on a field-emission scanning microscope (FESEM; Carl Zeiss Gemini Supra) operating at 10 kV. Transmission electron microscopy (TEM) images were recorded using a JEOL 2010F microscope operated at 200 kV. Raman spectra were obtained with a Super LabRam microscopic Raman

spectrometer. The wavelength of the exciting radiation provided by an inner air-cooled He−Ne laser was 632.8 nm.

To prepare the electrodes, the carbon nanocages were mixed thoroughly with polyvinylidene fluoride (PVDF) in a weight ratio of 95:5 in N-methyl-2-pyrrolidone (NMP). The mixtures were then pressed onto nickel mesh (100 mesh) as the working electrode. The electrode was dried at a temperature of 100 ºC under vacuum for approximately 24 hour. Li metal pressed on a nickel mesh was used as the reference and counter electrodes. Galvanostatic discharge–charge measurements were performed in 1 M $LiClO_4$ in EC-DEC (EC/DEC = 1/1, v/v) within voltage limits of 3.5-0.01 V (vs. Li^+/Li) under constant current densities of 0.1, 0.5, 1, 2, 5, and 10 A g^{-1}.

Results and discussion

Cage-like carbons are prepared by the catalytic decomposition of *p*-Xylene on a MgO supported Co/Mo catalyst in supercritical CO_2 at a pressure of 10.34 MPa over a temperature in the range from 650 to 750 ºC.[23] No obvious difference in the morphology of these carbon nanocages is observed in the SEM images as shown in Figure 1. In the reaction, the pyrolysis of *p*-Xylene occurs on the surface Co/Mo/MgO catalyst nanoparticles. The carbon

nanocages are obtained by the following dissolution of the Co/Mo/MgO catalyst in HNO_3. So the morphology of the catalyst determines the dimensions of the carbon nanocages. Given the fact that the same catalyst is used in the reaction, the carbon nanocages prepared at different temperatures exhibit the same spherical morphology.

Currently, carbon materials have been widely used as the electrode materials for lithium-ion batteries. The electrochemical performance of these electrode materials largely depends on the properties of the carbon materials, including the porosity, the specific surface area, the conductivity and morphology. Carbon with cage-like morphology is a promising candidate as electrodes for electrochemical applications. In order to demonstrate the potential application of these carbon nanocages as anodes, the Li insertion/extraction behavior of these materials have been investigated in this work. Figure 2 shows the first discharge/charge profiles of the nanocages of CNC-650, CNC-700, and CNC-750 at a discharge/charge rate of 0.1 A/g. As listed in Table 1, the first discharge and charge capacities of CNC-650 are 2504 and 627 mA h/g, respectively, comparable with those of mesoporous carbon CMK-3.[6] The discharge capacities of CNC-700 and CNC-750 are of 1397 and 1272 mA h/g, respectively, obviously lower than that of CNC-650. However, the reversible capacities of these carbon nanocages are in the same range, indicating that the irreversible capacity of CNC-650 is larger than those of CNC-700 and CNC-750. No obvious plateau is observed in the discharge

profiles of the carbon nanocages, similar to the typical carbon materials with low graphitization degree.[24,25] The slope between 0.9 and 0.5 V is ascribed to the formation of solid electrolyte interface (SEI).

The large irreversible capacity occurred in the first discharge/charge cycle is a common phenomenon for carbon materials, especially for hard carbon materials.[6,25-27] The irreversible capacity is originated from the formation of a SEI layer by the decomposition of the electrolyte on the electrode surface, and the reaction of Li with active sites in the electrode.[25,28] Thus, the irreversible capacity is related to the surface area and disorder degree of the electrode materials. As revealed in Table 1 and the following XRD, TEM and Raman investigations, compared with CNC-700 and CNC-750, CNC-650 has a higher specific surface area and a low graphitization degree. The high specific surface area and the low graphitization degree provide more active surface for the formation of the SEI layer and plenty of active sites for the irreversible reaction with Li ions, resulting in the large irreversible capacity.

Powder XRD diffraction technique is a useful tool to investigate the graphitization degree and disorder nature of carbon materials. The XRD pattern of CNC-750 shown in Figure 3 clearly exhibits two diffractions located at approximately 24.2, and 43.4 (2θ), corresponding to the (002) and (100) diffractions of graphite, respectively. The increase in the intensity of

the (002) diffractions with the reaction temperature and the absence of the (100) diffractions in the XRD patterns of CNC-650 and CNC-700 suggest that the graphitization degree of carbon nanocages prepared at 750 ^{o}C is higher than those prepared at lower temperatures, 650 and 700 ^{o}C. The *d*-spacing between the (002) planes of the carbon nanocages is approximately 0.37 nm, higher than the value of graphite. The large *d*-spacing and broadened diffraction peaks indicate that amorphous structures present in these carbon nanocages, even for the sample prepared at a temperature as high as 750 ^{o}C.

The structure and graphitization degree of these carbon nanocages are further revealed by the HRTEM observation. As shown in the HRTEM images in Figure 4, the thickness of the carbon shells are ranging from 2.0 to 3.0 nm for CNC-650, and from 4.0 to 5.0 nm for CNC-700 and CNC-750. The thicker carbon shells of CNC-700 and CNC-750 result from the faster pyrolysis rate of *p*-Xylene on the surface of the catalyst at elevated temperatures. The amorphous nature of CNC-650 is observed clearly in the HRTEM image (Figure 4a). The micropores presented in the carbon shell account for the high specific surface area of CNC-650. HRTEM image in Figure 4b reveals that the carbon nanocages CNC-700 are composed of curved carbon structure consisting of 5-10 carbon layers. However, no obvious graphite domains with ordered graphene sheets are observed, indicating that the graphitization degree of CNC-700 is still quite low. Higher graphitization degree is achieved by further

increasing the reaction temperature to 750 ^{o}C. As shown in Figure 4c, graphite domains are clearly observed in the carbon shell of CNC-750. The spacing among the graphene sheets is approximately 0.35 nm, consistent with the XRD investigation. The graphitization degree of the carbon nanocages prepared at different temperatures is also evaluated by the investigation on the vibration properties of the carbon structures by Raman technique. As shown in Figure 4d, all of the carbon nanocages exhibit two Raman peaks located at approximately 1336 and 1580 cm^{-1}, corresponding to the D- and G-band of polycrystalline carbon, respectively. The D-band is associated with the defects, curved sheets, dangling bonds in the carbon structures, and G-band corresponds to E_{2g} mode of graphite.[29] The higher intensity of the G-band of CNC-750 over that of CNC-600 and CNC-700 suggests the higher graphitization degree of CNC-750, consistent with the XRD and HRTEM observations.

The graphitization degree and porosity give an important impact on the coulombic efficiency of carbon materials. Low coulombic efficiency is expected for amorphous carbon with large specific surface area and low graphitization degree. As listed in Table 1, the coulombic efficiency of the first discharge-charge cycle is 25%, 36%, and 47% for CNC-600, CNC-700, and CNC-750, respectively. The variation in the coulombic efficiency of the first cycle is consistent with the nature of the carbon nanocages as revealed by the XRD, TEM, and Raman investigations. The coulombic efficiency variations of these carbon nanocages

are plotted as a function of the cycle number in Figure 5a. The coulombic efficiency of CNC-750 increases dramatically with discharge-charge cycles, reaching over 98% when discharge-charged for about 10 cycles. However, for CNC-700 and CNC-650, they have to be discharge-charged at the same current density for over 40 and 60 cycles, respectively, to gain such high coulombic efficiency.

The cycling stability during the Li insertion/extraction processes is an important factor for the successful application of carbon materials as electrodes for lithium-ion batteries. The cycling performance of the carbon nanocages is tested at a current density of 0.1 A/g. Figure 5b shows the profile of the charge capacities of the carbon nanocages varying with the discharge-charge cycles. The reversible capacities of CNC-650 decay gradually with the discharge-charge cycles. After discharge-charged for about 60 cycles, a reversible capacity of approximately 131 mA h/g is remained for CNC-650, only approximately 20 % of its initial charge capacity. Cycled at the same current density, the reversible capacities of CNC-750 is significantly higher than that of CNC-650. CNC-750 shows superb cycling stability. No obvious decay is observed for CNC-750 when discharge-charged for more than 60 cycles at a current density of 0.1 A/g. After 60 cycles, a reversible capacity of approximately 574 mA h/g, which is almost 96 % of its initial capacity, is well maintained for the CNC-750. CNC-700 also exhibits relatively good cycling stability, but lower reversible capacity. The

better cycleability of the carbon nanocages prepared at relatively higher temperatures is ascribed to the increased graphitization degree and lowered specific surface area. CNC-750 even shows higher reversible capacity and better cycling stability compared with hierarchically porous carbons,[25] the necklace-like hollow carbon nanospheres,[30] and carbon nanofilaments.[31]

Besides the high cycleability, the carbon nanocages prepared in supercritical CO_2 also exhibit promisingly high rate performance. Figure 6 shows the variations of the reversible capacities of the carbon nanocages with the current densities and discharge-charge cycles. The cells was first cycled at 0.1 A/g for 10 cycles, followed by the cycling at current densities increased stepwise to as high as 10 A/g. Compared with CNC-650 and CNC-700, CNC-750 exhibits superior rate performance. For CNC-750, a reversible capacity of approximately 400 mA h/g is achieved at a current density of 0.5 A/g, 235 mA h/g at 2.0 A/g and 58 mA h/g at 10 A/g. Once the current density lowered back to 0.1 A/g, a reversible capacity of 510 mA h/g is restored, indicating the good reversibility of these carbon nanocages. Cycling at a current density of 2.0 A/g, reversible capacities of approximately 85 and 75 mA h/g were obtained for CNC-650 and CNC-700, respectively, much lower than that of CNC-750. It is surprising to note that cycled at current densities over 1.0 A/g, the reversible capacity of CNC-650, which has high specific surface area and low graphitization degree is comparable

to that of CNC-700. Given the high specific surface area, the energy might be stored in the carbon nanocages following a mechanism similar to the electric double-layer capacitor (EDLC) when cycled at high rate. Due to the significant contribution of the energy stored by EDLC, the capacity of CNC-650 at rates over 1.0 A/g is higher than that of CNC-700. The current density of 10 A/g is too high for CNC-650 and CNC-700 to get satisfactory reversible capacities, indicating the poor rate performance of these carbon nanocages. It is also noted that the higher the current density, the better the cycleability, consistent with the hierarchically porous carbon monoliths reported in the literature.[25].

The high reversible capacities and superior rate performance of the carbon nanocages prepared by the supercritical fluid method in this work are ascribed to the unique structure of these carbon nanocages which favors both the electron transportation and electrolyte penetration (as illustrated in Figure 7). First, the highly graphitized carbon shell and the well contacted cages ensure the fast and continuous transportation of electrons. Second, the unique porous structure of the carbon electrodes provides a pathway for the fast distribution of the electrolyte and ions. N_2 adsorption-desorption analyses of these carbon nanocages reveal the presence of fine pores,[23] with a mean diameter of about 2.3 nm, and large mesopores, with a mean diameter of approximately 20 nm, probably resulting from the opening in the carbon shell and the inter-cage space among the cages. The dissolution of the

catalyst inside the cages by the HNO_3 acid also indicate that pore channels, which work as the pathway for the acid, exist in the carbon shell. The large inter-cage mesopores, together with the fine pores in the cage shell form a network, facilitating the diffusion of electrolyte into the cages, and thus the fast transportation of the ions. Third, the readily accessed void space inside the cages works as a reservoir for the electrolyte, leading to efficient Li insertion into the carbon shells from both the outer and inner surface of the cages. Moreover, the shell thickness of these carbon nanocages is only several nanometers, greatly shortened the diffusion distance of Li ions. The fast electron transportation among the well-graphitized carbon nanocages, the efficient electrolyte penetration in the porous network, and the shorten Li diffusion distance in the thin carbon shells might account for the high electrochemical performance of the carbon nanocages.

Conclusion

Carbon nanocages have been prepared by a catalytic decomposition of *p*-Xylene in supercritical CO_2 at a pressure of 10.34 MPa and temperatures ranging from 650 to 750 ^oC. Due to the high graphitization degree of the carbon shells, the carbon nanocages prepared at a temperature of 750 ^oC exhibited better electrochemical performance than those prepared at temperatures of 650 to 700 ^oC. The high reversible capacities, superior rate performance,

and good cycleability of the carbon nanocages prepared in this work are ascribed to the unique structure of these carbon nanocages. The well-contacted carbon nanocages with fine pores in the thin carbon shells ensure the fast electron transportation among the well-graphitized carbon nanocages, the efficient electrolyte penetration in the porous network, and the shorten Li diffusion distance in the thin carbon shells.

Acknowledgement

This work was supported by the National Natural Science Foundation of China (20731003, 20901050), and Shanghai Pujiang Program (09PJ1405700).

References

(1) Beguin, F.; Metenier, K.; Pellenq, R.; Bonnamy, S.; Frackowiak, E. *Mol. Cryst. Liquid Cryst.* **2000**, *340*, 547.

(2) Flandrois, S.; Simon, B. *Carbon* **1999**, *37*, 165.

(3) Kaskhedikar, N. A.; Maier, J. *Adv. Mater.* **2009**, *21*, 2664.

(4) Wang, Q.; Li, H.; Chen, L. Q.; Huang, X. J. *Carbon* **2001**, *39*, 2211.

(5) Wu, Y. P.; Rahm, E.; Holze, R. *J. Power Sources* **2003**, *114*, 228.

(6) Zhou, H. S.; Zhu, S. M.; Hibino, M.; Honma, I.; Ichihara, M. *Adv. Mater.* **2003**, *15*, 2107.

(7) Levi, M. D.; Aurbach, D. *J. Phys. Chem. B* **1997**, *101*, 4641.

(8) Wang, Q.; Li, H.; Huang, X. J.; Chen, L. Q. *J. Electrochem. Soc.* **2001**, *148*, A737.

(9) Frackowiak, E.; Beguin, F. *Carbon* **2002**, *40*, 1775.

(10) Frackowiak, E.; Gautier, S.; Gaucher, H.; Bonnamy, S.; Beguin, F. *Carbon* **1999**, *37*, 61.

(11) Frackowiak, E.; Jurewicz, K.; Delpeux, S.; Beguin, F. *J. Power Sources* **2001**, *97-8*, 822.

(12) Frackowiak, E.; Metenier, K.; Bertagna, V.; Beguin, F. *Appl. Phys. Lett.* **2000**, *77*, 2421.

(13) Leroux, F.; Metenier, K.; Gautier, S.; Frackowiak, E.; Bonnamy, S.; Beguin, F. *J. Power Sources* **1999**, *81*, 317.

(14) Rosolen, J. M.; Matsubara, E. Y.; Marchesin, M. S.; Lala, S. M.; Montoro, L. A.; Tronto, S. *J. Power Sources* **2006**, *162*, 620.

(15) Wu, G. T.; Wang, C. S.; Zhang, X. B.; Yang, H. S.; Qi, Z. F.; He, P. M.; Li, W. Z. *J. Electrochem. Soc.* **1999**, *146*, 1696.

(16) Kim, Y. A.; Kojima, M.; Muramatsu, H.; Umemoto, S.; Watanabe, T.; Yoshida, K.; Sato, K.; Ikeda, T.; Hayashi, T.; Endo, M.; Terrones, M.; Dresselhaus, M. S. *Small* **2006**, *2*, 667.

(17) Claye, A. S.; Fischer, J. E.; Huffman, C. B.; Rinzler, A. G.; Smalley, R. E. *J. Electrochem. Soc.* **2000**, *147*, 2845.

(18) Gao, B.; Bower, C.; Lorentzen, J. D.; Fleming, L.; Kleinhammes, A.; Tang, X. P.; McNeil, L. E.; Wu, Y.; Zhou, O. *Chem. Phys. Lett.* **2000**, *327*, 69.

(19) Park, M. S.; Needham, S. A.; Wang, G. X.; Kang, Y. M.; Park, J. S.; Dou, S. X.; Liu, H. K. *Chem. Mater.* **2007**, *19*, 2406.

(20) Zhou, H. S.; Zhu, S. M.; Hibino, M.; Honma, I. *J. Power Sources* **2003**, *122*, 219.

(21) Xing, W.; Bai, P.; Li, Z. E.; Yu, R. J.; Yan, Z. F.; Lu, G. Q.; Lu, L. M. *Electrochim. Acta* **2006**, *51*, 4626.

(22) Wang, T.; Liu, X. Y.; Zhao, D. Y.; Jiang, Z. Y. *Chem. Phys. Lett.* **2004**, *389*, 327.

(23) Li, Z. L.; Jaroniec, M.; Papakonstantinou, P.; Tobin, J. M.; Vohrer, U.; Kumar, S.; Attard, G.; Holmes, J. D. *Chem. Mater.* **2007**, *19*, 3349.

(24) Adelhelm, P.; Hu, Y. S.; Chuenchom, L.; Antonietti, M.; Smarsly, B. M.; Maier, J. *Adv. Mater.* **2007**, *19*, 4012.

(25) Hu, Y. S.; Adelhelm, P.; Smarsly, B. M.; Hore, S.; Antonietti, M.; Maier, J. *Adv. Funct. Mater.* **2007**, *17*, 1873.

(26) Zhang, J.; Hu, Y. S.; Tessonnier, J. P.; Weinberg, G.; Maier, J.; Schlogl, R.; Su, D. S. *Adv. Mater.* **2008**, *20*, 1450.

(27) Lee, K. T.; Lytle, J. C.; Ergang, N. S.; Oh, S. M.; Stein, A. *Adv. Funct. Mater.* **2005**, *15*, 547.

(28) Matsumura, Y.; Wang, S.; Mondori, J. *J. Electrochem. Soc.* **1995**, *142*, 2914.

(29) Dresselhaus, M. S.; Dresselhaus, G.; Pimenta, M. A.; Eklund, P. C. In *Analytical Applications of Raman Spectroscopy*; Pelletier, M. J., Ed.; Blackwell Science: Oxford, U. K., 1999; Chapter 9.

(30) Wu, C. Z.; Zhu, X.; Ye, L. L.; OuYang, C. Z.; Hu, S. Q.; Lei, L. Y.; Xie, Y. *Inorg. Chem.* **2006**, *45*, 8543.

(31) Habazaki, H.; Kiriu, M.; Konno, H. *Electrochem. Commun.* **2006**, *8*, 1275.

Captions

Figure 1 SEM images carbon nanocages prepared in sc-CO_2 at (a) 650, (b) 700, and (c) 750 ^oC.

Figure 2 The first discharge-charge profiles of the carbon nanocages at a current density of 0.1 A/g.

Figure 3 The powder XRD patterns of (a) CNC-650, (b) CNC-700, and (c) CNC-750.

Figure 4 HRTEM images of (a) CNC-650, (b) CNC-700, (c) CNC-750, and (d) Raman spectra of these carbon nanocages. The high magnification TEM image of CNC-750 (inset in c) shows the graphene sheets in the carbon shell.

Figure 5 (a) Coulombic efficiencies and (b) cycling performances of the carbon nanocages.

Figure 6 Rate performances of the carbon nanocages.

Figure 7 Schematic representations of electron transportation and Li ion diffusion in the carbon shell, and electrolyte penetration within the porous network of the carbon nanocages.

Table 1 The specific surface area of the carbon nanocages determined by N_2 adsorption-desorption, and the first cycle discharge, charge capacity and coulombic efficiency of these carbon nanocages discharge-charged at a current density of 0.1 A/g.

	Temperature (^oC)	S_{BET} (m^2/g)	1st Discharge Capacity (mA h/g)	1st Charge Capacity (mA h/g)	Coulombic Efficiency (%)
CNC-650	650	1240	2504	627	25
CNC-700	700	698	1397	460	36
CNC-750	750	680	1271	598	47

Figure 1

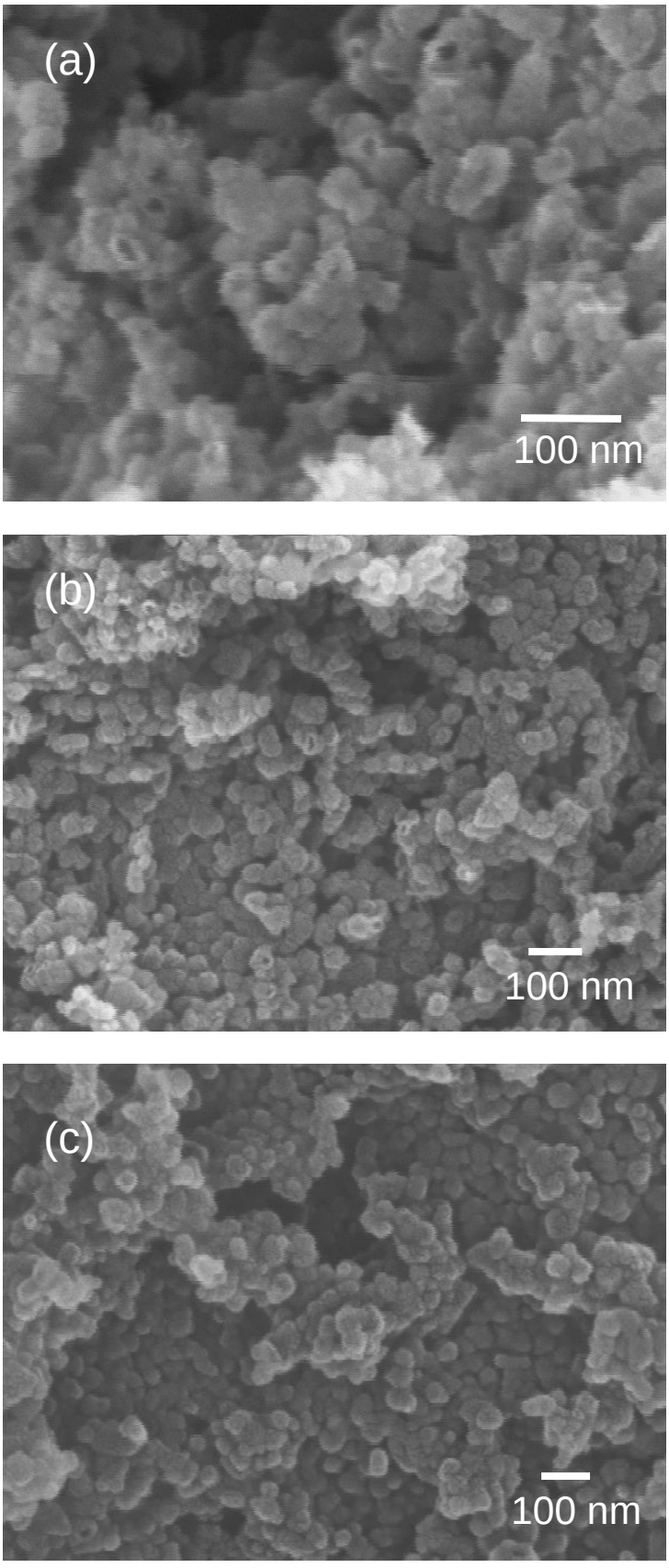

Figure 2

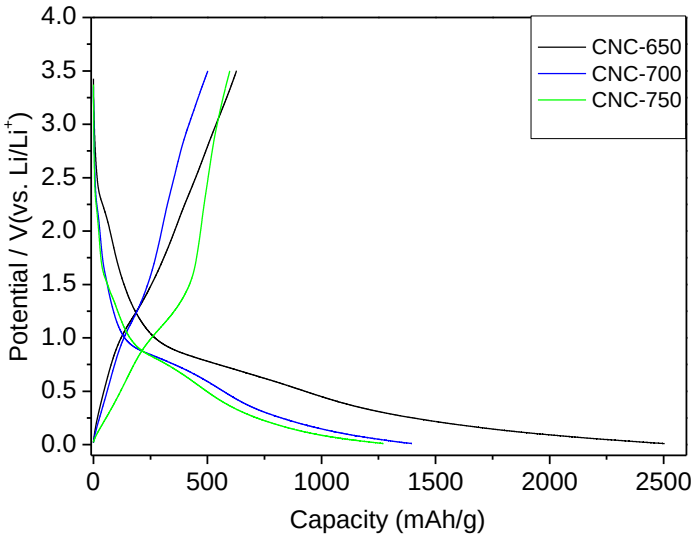
CNC-650
CNC-700
CNC-750
Potential / V(vs. Li/Li+)
Capacity (mAh/g)
4.0
3.5
3.0
2.5
2.0
1.5
1.0
0.5
0.0
0
500
1000
1500
2000
2500

Figure 3

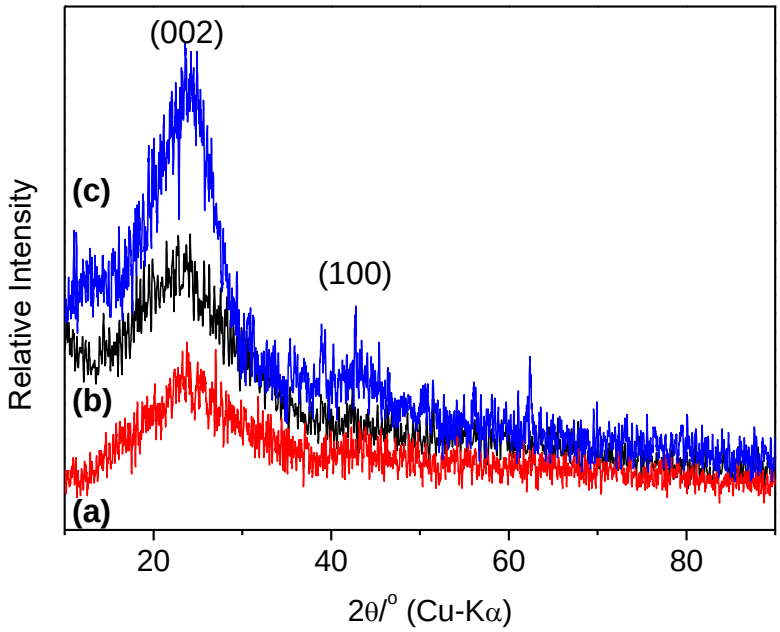

Figure 4

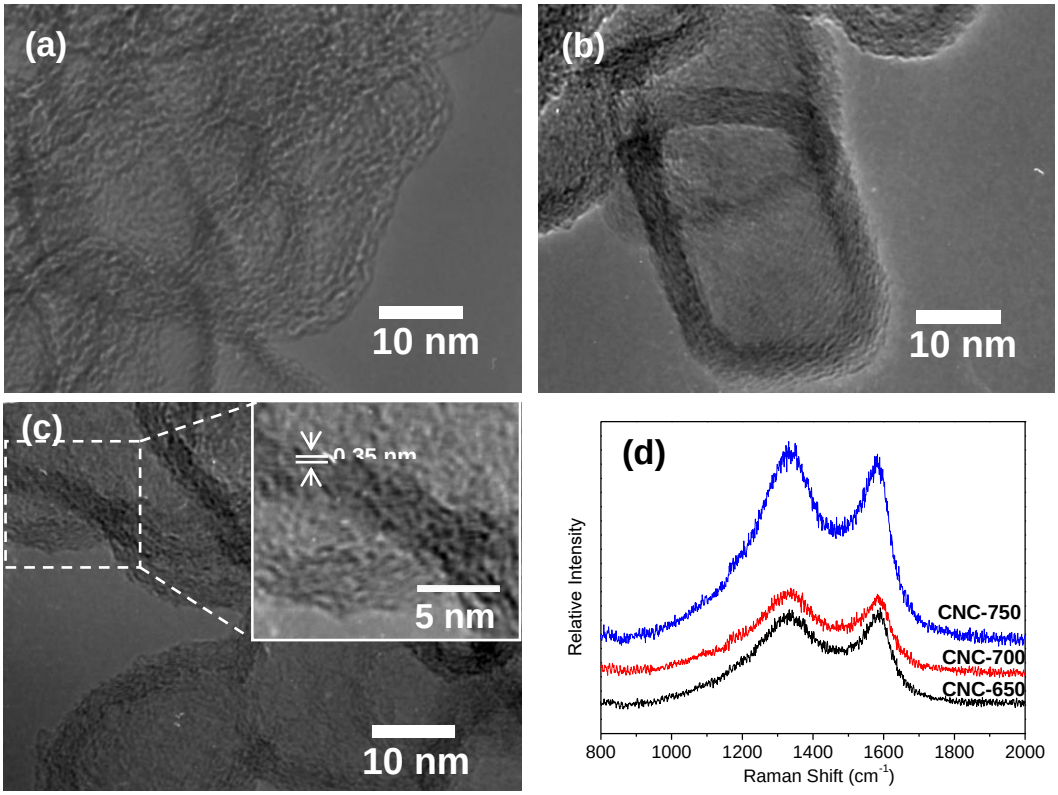
(a)
10 nm
(b)
10 nm
(c)
0.35 nm
5 nm
10 nm
(d)
Relative Intensity
CNC-750
CNC-700
CNC-650
800
1000
1200
1400
1600
1800
2000
Raman Shift (cm-1)

Figure 5

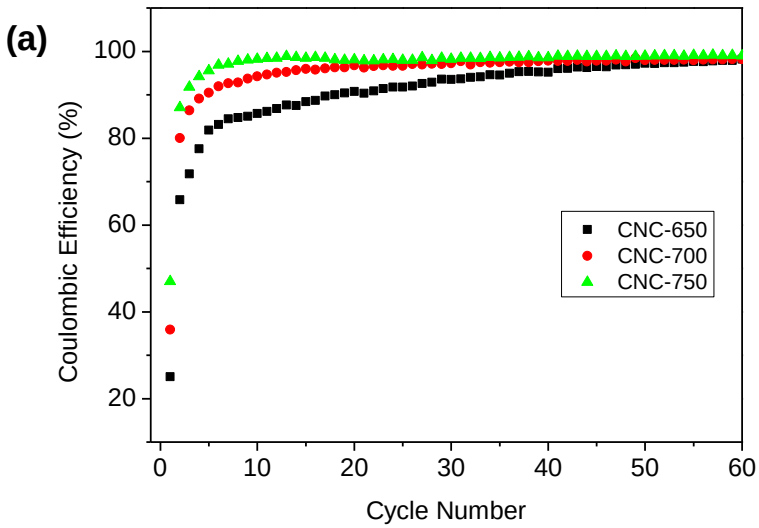
(a)
Coulombic Efficiency (%)
Cycle Number
CNC-650
CNC-700
CNC-750

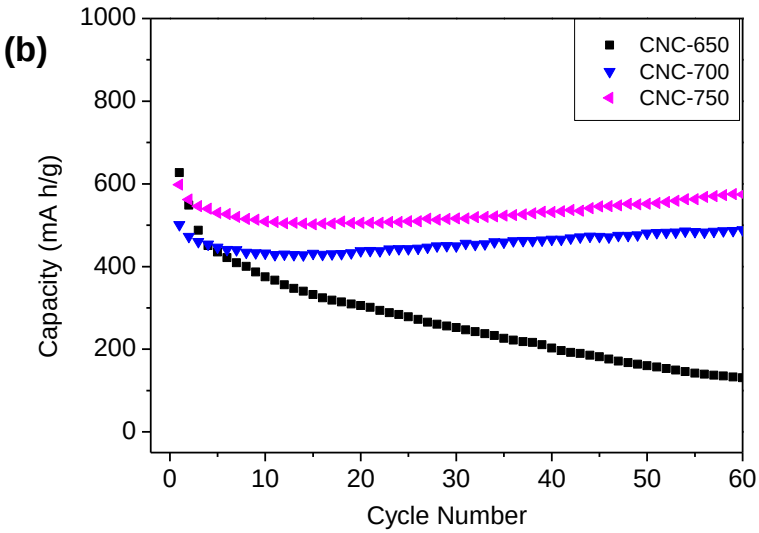
(b)
Capacity (mA h/g)
Cycle Number
CNC-650
CNC-700
CNC-750

Figure 6

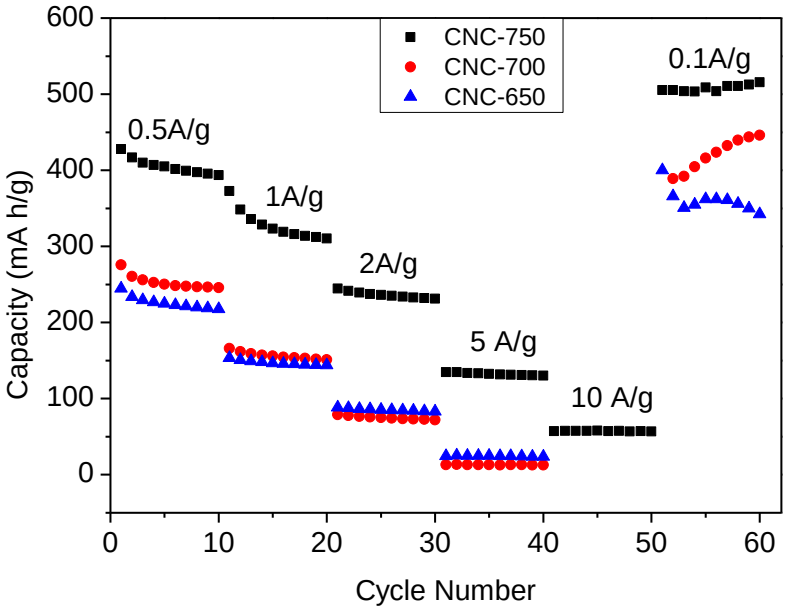
CNC-750
CNC-700
CNC-650
0.5A/g
1A/g
2A/g
5 A/g
10 A/g
0.1A/g
Capacity (mA h/g)
Cycle Number
0
100
200
300
400
500
600
0
10
20
30
40
50
60

Figure 7

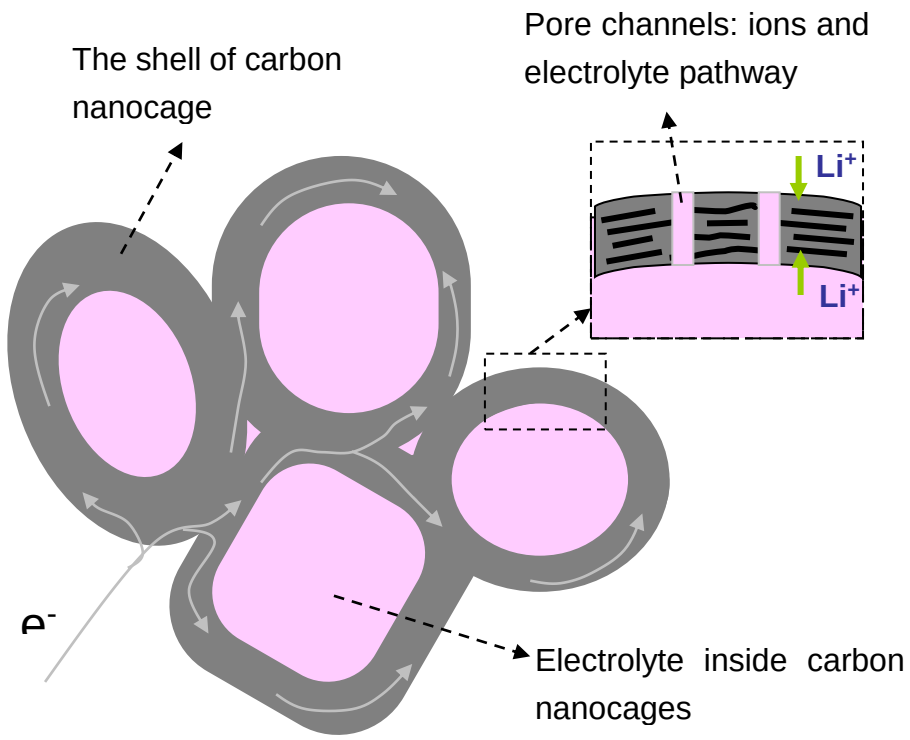
Pore channels: ions and electrolyte pathway
The shell of carbon nanocage
Li+
Li+
e-
Electrolyte inside carbon nanocages